# Journal of Materials Chemistry A

Accepted Manuscript


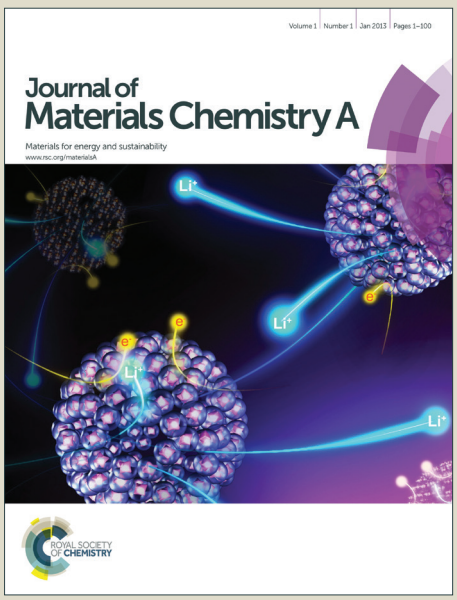





ROYAL SOCIETY OF CHEMISTRY

www.rsc.org/materialsA

Cite this: DOI: 10.1039/c0xx00000x

www.rsc.org/xxxxxx

ARTICLE TYPE

# Sn-doped Hematite Film as Photoanode for Efficient Photoelectrochemical Water Oxidation

**Dong-Dong Qin,*[a] Yun-Lei Li,[a] Ting Wang,[a] Yang Li,[a] Xiao-Quan Lu,[a] Jing Gu,[b] Yi-Xin Zhao,[c] Yu-Min Song*[a] and Chun-Lan Tao*[d]**

***Received (in XXX, XXX) Xth XXXXXXXXX 20XX, Accepted Xth XXXXXXXXX 20XX***

**DOI: 10.1039/b000000x**

**Sn-doped hematite film was electrochemically deposited on the fluorine-doped tin oxide substrate as anode for photoelectrochemical water oxidation. The high photocurrent of ~2.8 mA·cm$^{-2}$ at 1.24 V vs RHE and the conversion efficiency of 0.24 % are achieved.**

To satisfy the increasing global energy demand, photoelectrochemical water splitting has been considered to be one of the promising strategies to transform solar energy into fuels in the form of hydrogen.[1] As the key part of the photoelectrochemical cell, numerous n-type semiconductor metal oxides such as $TiO_2$,[2] $WO_3$,[3] α-$Fe_2O_3$[4] and p-type semiconductor such as $Cu_2O$,[5] $CuRhO_2$[6] have been developed to drive desired reactions. Given that a superior semiconductor electrode should be composed of inexpensive and abundant elements and should remain highly stable during photoelectrochemical reaction, hematite, an n-type semiconductor with a bandgap of 2.1 eV and the appropriate valence band position for $O_2$ evolution is a promising photoanode material.[7] However, hematite suffers from short hole diffusion length, slow water oxidation kinetics and low conductivity,[8] one prospective solution to overcome these drawbacks are fabrication of nanostructured materials and impurity doping with Ti, Si and Sn et al.[9]

To date, Sn-doped hematite has been widely studies due to the relatively high chemical stability of Sn precursors (such as $SnCl_2$ and $SnCl_4$) and thus easy operation during doping. Various techniques, including electrochemical deposition,[10]flame annealing,[11]coevaporating iron and tin in a reacative oxygen ambient,[12] hydrothermal and high temperature annealing,[13] have been used to fabricate hematite film with controllable Sn content. However, none of them demonstrate a photocurrent more than 1.9 mA·cm$^{-2}$ at 1.23 V vs RHE, although the photoelectrochemical performance of doped samples are indeed improved as compared with pristine hematite. Among these techniques, electrochemical deposition does not need costly manufacturing equipment and harsh condition for film growth.[14] Most importantly, the film with desired thickness can be grown within short time, usually less than half hour. These features endow electrochemical deposition great advantages to prepare efficient electrode for the application in photoelectrochemical water splitting.[15]

Here, we report the synthesis of hematite film on FTO substrate by facile electrochemical deposition method, followed by studying the influence of parameters such as Sn concentration, annealing temperature, time of deposition on the performance of samples. Under full light irradiation of AM 1.5 G, 100 mW·cm$^{-2}$, the optimized sample exhibits an anode photocurrent as high as 2.8 at 1.24 V vs RHE and 4.6 mA·cm$^{-2}$ before the onset of the dark current, which corresponds to a total conversion efficiency of 0.24%. We believe that the excellent photoresponse of the sample is due to the improved conductivity, charge transfer and water oxidation kinetics as a result of increased carrier density and surface modification with $Co^{2+}$.

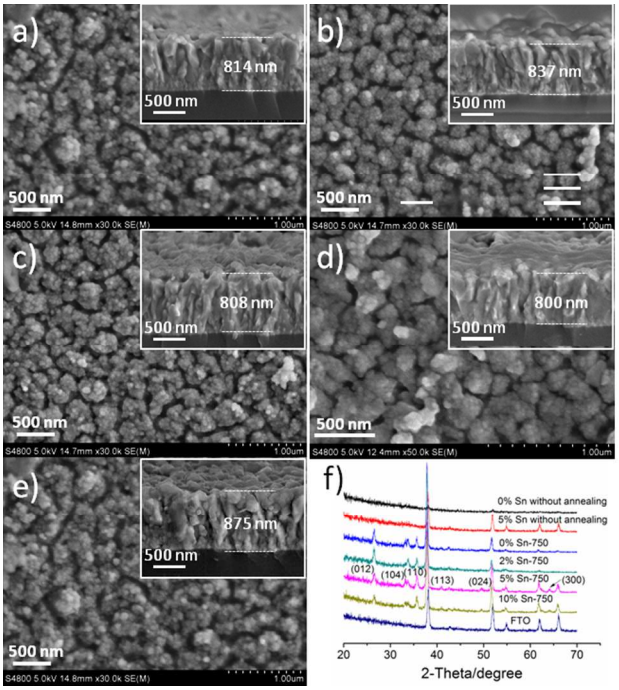


**Fig.1** FE-SEM images of hematite films on FTO: (a, b, c and d) samples annealed at 750 °C , with 0%, 2%, 5% and 10% Sn doping, respectively, e) 5% Sn doped, before annealing, f) XRD patterns of the samples. Insert is the cross sectional view of the samples.

Electrochemcial deposition of hematite films were conducted using a standard three-electrode cell, with FTO as working electrode, Pt foil as counter electrode and SCE as reference. A solution contains 5 mM $FeCl_3·6H_2O$, 5 mM NaF, 0.1 M KCl, 1M $H_2O_2$ and x% $SnCl_2·H_2O$ (where x is the molar ratio of Sn to Fe,

x% = 0, 2, 5, and 10) as deposition solution. Deposition was carried out at 50 ºC by applying 100 potential cycles between -0.2 to 0.4 V vs SCE at a scan rate of 200 mV·s$^{-1}$. The as-prepared films were rinsed with DI water and annealed at different temperature. The morphologies of the film deposited on the FTO substrate after Sn doping or annealing were checked by FE-SEM. As shown in Fig. 1a-e, all the samples show uniform and continuous film with no obvious aggregation on the surface. Incorporation of Sn element into the lattice of hematite does not induce significant changes in the surface morphology except for the heavily doped sample with 10% Sn, in which the feature size of the particulate shape increase slightly as can be seen from Fig. 1d. The thickness of 800-875 nm for all the samples are observed after verifying by the cross sectional view of SEM images. Judging from Fig. 1c and e, a little shrink of about 70 nm in film thickness occurs after being annealed at 750 ºC for 30 min.

The crystal structure and the possible phase change of sample during thermal annealing were examined by X-ray diffraction. As illustrated in Fig. 1f, the as-prepared samples are amorphous phase, with no clear diffraction peaks of the hematite. It crystallizes into hexagonal hematite structure after annealing at 750 ºC, as confirmed by appearance of diffraction peaks of (012), (104), (110) (113), (024) and (300). The doped samples show no observable shifts of all characteristic diffraction peaks compared to pristine hematite film, suggesting the main crystal structure is preserved during doping. Raman spectra have been shown in Fig. S1 to characterize the composition of hematite films. Five of seven possible optical modes (2Ag+5Eg) for hematite are observed with correspondence: Ag, 226 and 500 cm$^{-1}$, and Eg, 292, 410 and 610 cm$^{-1}$.[16] An extra peak appeared at 656 cm$^{-1}$ can be assigned to the presence of magnetite ($Fe_3O_4$), which has been found in those hematite films prepared by electrochemical deposition.[17] No obvious peaks are observed for unannealed samples except for the weak signals arising from FTO substrate. This is probably due to the low crystallinity of the as-prepared samples, as evidenced by the XRD data. In order to investigate the state of Sn in the samples, XPS measurements were conducted. From XPS data shown in Fig S2, it is found that Sn element exists in the samples of 5% Sn as-prepared, 5% Sn-750 ºC and 0% Sn-750 ºC. This result clearly shows that: 1) the electrochemical deposition method is effective to incorporate Sn element into hematite film; 2) the state of Sn element in all the samples tested is four plus; 3) high temperature annealing can induce Sn diffusion from FTO substrate into hematite film.

The UV-vis spectra, photoluminescence spectra and Time-Correlated Single Photon Counting were measured to characterize the hematite films. The band gap is estimated to be 2.16, 2.16 and 2.15 eV from UV-vis spectra in Fig. S3 for samples of 5% Sn-750 ºC, 0% Sn-750 ºC and 5% Sn-as prepared, respectively. These values are comparable with those reported hematite.[9] From photoluminescence spectra illustrated in Fig. S4, it can be seen that as-prepared sample exhibits higher photoluminescence than those being annealed at 750 ºC, indicating high carrier recombination rate of unannealed samples. Compared with 0% Sn-750 ºC sample, the weaker photoluminescence of 5% Sn-750 ºC sample implies lowered electro-hole recombination. Accordingly, the 5% Sn-750 ºC sample shows extended photoluminescence lift time of 1.2258 ns among the samples measured by the Time-Correlated Single Photon Counting, as shown in Fig. S5.

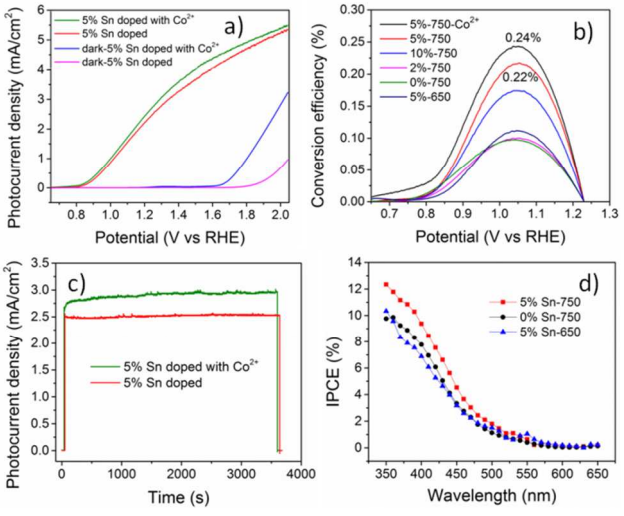


**Fig.2** a) Photocurrent response, b) conversion efficiency, c) long-term stability assay and d) IPCE of the samples measured at 1.2 V vs RHE.

Photoelectrochemcial performance of the samples were investigated by linear sweep voltammograms under AM 1.5 G (100 mW·cm$^{-2}$) illumination in 1.0 M NaOH. Previous research reveals that high temperature annealing can induce Sn diffusion from FTO substrate to hematite film and high temperature annealing is also necessary to activate the Sn doped hematite prepared at low temperature. Both process can benefit to the successful doping and thus generate high photocurrent. Hence, a high annealing temperature of 750 ºC is employed to maxim the performance of the hematite in this work. As shown in Fig. 2a and Fig. S6, for 750 ºC annealed samples the photocurrent increase with the elevated Sn concentration in deposition solution from 0%, 2% to 5% (molar ratio of Sn to Fe). However, continuing increase Sn concentration to 10% results in a significant decrease of the photocurrent. A satisfactory photocurrent up to 2.5 mA·cm$^{-2}$ at 1.24 V vs RHE and 4.6 mA·cm$^{-2}$ before the onset of the dark current are obtained for 5% Sn doped samples, corresponding to a total conversion efficiency of 0.22% (see Fig. 2b). These values increased to 2.8 mA·cm$^{-2}$ at 1.24 V vs RHE, with a conversion efficiency of 0.24%, after being treated with an oxygen evolution catalysts $Co^{2+}$. These photocurrent and conversion efficiency are fairly superior for hematite photoanode, but still lower than a $IrO_2$ modified cauliflower-like hematite[18] and a silicon/hematite heterojunction material.[19] It is not uncommon that the improved performance for $Co^{2+}$ modified sample was gained, due to accelerated water oxidation kinetic,[20] which is known as one of the restraining factor for hematite to achieve high photocurrent.

Fig. 2c shows long-term stability of 5% Sn doped sample before and after $Co^{2+}$ modification. It can be seen that both samples exhibit decent stability and retain almost 100% of their photocurrent after 1h illumination at a bias of 1.24 V vs RHE. Additionally, It was found that the photocurrent of 5% Sn doped samples increase remarkably from 0.03 to 1.1 and finally to 2.5 mA·cm$^{-2}$ when annealed at 500, 650 and 750 ºC, respectively, reflecting the importance of annealing temperature. The higher photocurrent of 0% doped, 750 ºC annealed sample than the one

of 5% Sn doped, 650 ºC annealed implies the Sn diffusion from substrate to hematite occurs. Then, we checked the effects of deposition duration time on the photoresponse of the samples. The results illustrated in Fig. S7a indicate that the film with 10 min. (100 potential cycle) deposition has the highest photocurrent of 2.5 mA·cm$^{-2}$. The deposition time either shorter or longer than that leads to a greatly decrease of photocurrent. At last, it was found that ramp rate of annealing is also a critical factor determining the photoelectrochemical performance of the samples as shown in Fig. S7b. The heating rate of 10 ºC per minute is the best. The relatively high heating rate possesses the benefits of: 1) avoiding loss conductivity of FTO due to exposure at high temperature for long time; 2) achieving faster Sn diffusion and doping with a more even distribution before the transformation to highly crystalline hematite occurs. A higher heating rate of 15 ºC per minute, we assume, may cause insufficient Sn doping and consequently, leading to poor photoresponse. The IPCE values in Fig. 2d shows photocurrent cut off edge of about 600 nm, reflecting the band gap of approximately 2.1 eV for hematite, consistent with the results obtained from optical spectra.

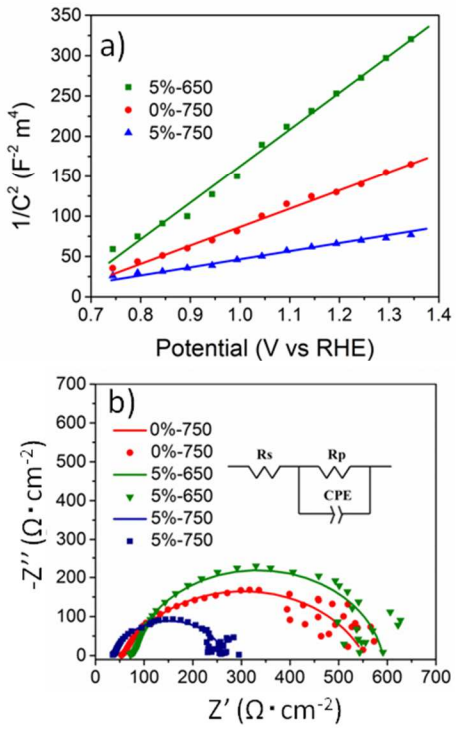


**Fig.3** a) Mott-Schottky plots of the hematite films obtained in 1.0 M NaOH solution in the dark, b) Nyquist plots of the hematite films under an illumination of AM 1.5G light (50 mW·cm$^{-2}$), in 1.0 M NaOH solution at a bias of 1.54 V vs RHE. Solid dots represent experimental data, and the line represents model values.

In order to understand the roles of the annealing temperature and molar ratio of Sn to Fe on the electronic properties of the hematite films, the Mott-Schottky method and Nyquist plots are used to determine the flat band potential ($E_{fb}$) and carrier density. The flat band potential determined by Mott-Schottky method illustrated in Fig. 3a shows that the estimated $E_{fb}$ are 0.64, 0.60 and 0.48 V vs RHE for 5%, 0% and 5% Sn doped samples annealed at 650, 750 and 750 ºC, respectively. These values are comparable to the Sn doped hematite nanowires reported by us previously.[21] In theory, the flat band potential should be approximately equal to the onset potential. However, as shown in Fig. S8, the same onset potential of about 0.69 V for three samples are observed from chopped light IV curve, which are obviously not in accordance with its flat band potential estimated. The positive shifts of the onset potential may be attributed to the high recombination of photo-generated carriers and slow oxygen evolution kinetics at the surface of the hematite. Therefore, an oxygen evolution catalyst $Co^{2+}$ is modified onto the surface of hematite. Given that hematite film prepared is nanostructured and part of the FTO may be exposed to the electrolyte, generally used electrochemical deposition would grow Co-Pi on the FTO substrate preferentially because of its high conductivity. In this case, unwanted dark current will increase due to the back flow of the electrons from the back contact. Hence, a dip coating method is employed through soaking samples in the $Co(NO_3)_2$ solution. The results shown in Fig. S8 reveal a clear negative shift of onset potential from 0.69 to 0.49 V for 750 ºC annealed sample with 5% Sn doping after $Co^{2+}$ modification. This value of onset potential is already very close to its flat band potential estimated from Mott-Schottky plots, implying effective contribution of $Co^{2+}$ modification on improvement of oxygen evolution kinetics. The increased photocurrent observed in Fig. 1a confirms the hypothesis.

The positive slop of the Mott-Schottky plots indicates Sn-doped hematites belong to n-type semiconductor, consistent with that observed in Ti and Si doped hematite. But differs from the Zn doped hematite,[22] from which a unique p-type doping is seen. The electron density is calculated to be $3.88\times10^{19}$, $7.86\times10^{19}$ and $1.95\times10^{20}$ cm$^{-3}$ for 5%, 0% and 5% Sn doped samples annealed at 650, 750 and 750 ºC, respectively. The values are in the range of those found for Ni doped hematite[23] but lower than Ti doped hematite.[24] It is noted that photocurrent for those samples increase monotonically with their electron donor density. To clarify this, we think that four plus metal doping can lead to changes of oxygen stoichiometry in hematite lattice or formation of $Fe^{2+}$ sites to balance charge,[25] either of which can improve the conductivity of the sample. This hypothesis can also be concluded from the equation $\sigma = ne_0\mu_0$. As a result of increased conductivity, two factors may contribute to the higher photocurrents seen at higher electron donor density: 1) lowered recombination rate and faster collection of the photo-generated electrons at the back contact; 2) decreased thickness of space charge layer with higher electric field drive force to effective separation and transport of electrons and holes.

Nyquist plots are measured to supply more evidences under illumination of AM 1.5G light, 50 mW·cm$^{-2}$, with a bias of 1.54 V vs RHE. The experimental data are fitted well by use an equivalent circuit Rs(CPE-Rp), where Rs is the ohmic contribution, CPE is the constant phase element that takes into account non-idealities in the capacitance of the Helmholtz layer, and Rp is the charge transfer resistance. In this model, the low frequency response is assigned to the charge transfer resistance. In contrast, the response at high frequency is relatively small, implying fast electronic process in the semiconductor. Therefore, the smaller the semicircle is, the faster the charge transfer rate of

photogenerated charge carriers. As shown in Fig. 3b, the smallest semicircle for 5% Sn doped, 750 ºC annealed sample is seen, consistent with its highest photocurrent among the samples discussed. This result provides direct evidence that the excellent performance of the samples are probably attributed to the elevated donor density by appropriate concentration of Sn doping and improved conductivity, resulting in efficient charge separation and transportation.

## Conclusions

In summary, we have synthesized Sn-doped hematite film on FTO substrate using a facile electrochemical deposition method with short duration time of 10 min. From optimization of parameters such as electrodeposition time, annealing temperature and procedure, concentration of Sn doping and surface modification with an oxygen evolving catalyst, the high anode photocurrent up to 2.8 at 1.24 V vs RHE and 4.6 mA·cm$^{-2}$ before the onset of the dark current, corresponding to a total conversion efficiency of 0.24% are achieved. The excellent photoresponse of the samples, we believe, is due to the improved conductivity, charge transfer and water oxidation kinetics as a result of increased carrier density and surface modification with $Co^{2+}$. Additionally, we find in this work that heating rate of annealing greatly influence the performance of the hematite grown on FTO, due to the balance between conductivity of substrate and the appropriate concentration of doping needed. The electrochemical deposition is proved to be an effective method to fabricate high performance Sn-doped hematite, it may also be working to prepare doped hematite with other elements or other materials with or without doping.

## Acknowledgements

This work was financially supported by National Natural Science Foundation of China for Young Scholars (no. 21401150), Natural Science Foundation of Gansu Province (no. 1308RJYA043), Science and Technology Support Program of Gansu Province (no.1304GKCA038), Scientific Capability Promoting Project for Young Teachers in Northwest Normal University (NWNU-LKQN-13-7), Fundamental Research Funds for the Central Universities (no. lzujbky-2014-39) and the Program for Chang Jiang Scholars and Innovative Research Team, Ministry of Education of China (no. IRT1283).

## Notes and references

[a]*Key Lab of Bioelectrochemistry and Environmental Analysis of Gansu, College of Chemistry and Chemical Engineering, Northwest Normal University, Lanzhou, Gansu 730070, People's Republic of China. E-mail: qindd05@gmail.com(D.-D Qin), songym@nwnu.edu.cn(Y.-M Song)*

[b]*Department of Chemistry, Princeton University, Princeton, New Jersey 08544, United States*

[c]*School of Environmental Science and Engineering, Shanghai Jiao Tong University, 200240, People's Republic of China*

[d]*School of Physical Science and Technology, Lanzhou University, Lanzhou, Gansu 730000, People's Republic of China, E-mail: taochl@lzu.edu.cn(C.-L Tao)*

† Electronic Supplementary Information (ESI) available: other details are given in the supporting information. See DOI: 10.1039/b000000x/

1 M. Grätzel, *Nature* 2001, **414**, 338. W. J. Youngblood, S. H. A. Lee, K. Maeda and T. E. Mallouk, *Acc. Chem. Res*. 2009, **42**, 1966.

2 A. Fujishima and K. Honda, *Nature*, 1972, **238**, 37.

3 D. D. Qin, C. L. Tao, S. A. Friesen, T. H. Wang, O. K. Varghese, N. Z. Bao, Z. Y. Yang, T. E. Mallouk and C. A. Grimes, *Chem. Commun*., 2012, **48**, 729. H. C. He, S. P. Berglund, P. Xiao, W. D. Chemelewski, Y. H. Zhang and C. B. Mullins, *J. Mater. Chem. A*, 2013, **1**, 12826.

4 K. Sivula, F. Le Formal and M. Grätzel, *ChemSusChem*, 2011, **4**, 432. Y. Lin, G. Yuan, S. Sheehan, S. Zhou and D. Wang, *Energy Environ. Sci*. 2011, **4**, 4862. A. B. F. Martinson, M. J. DeVries, J. A. Libera, S. T. Christensen, J. T. Hupp, M. J. Pellin and J. W. Elam, *J. Phys. Chem. C*, 2011, **115**, 4333.

5 A. Paracchino, V. Laporte, K. Sivula, M. Grätzel and E. Thimsen, *Nature materials*, 2011, **10**, 456.

6 J. Gu, Y. Yan, J. W. Krizan, Q. D. Gibson, Z. M. Detweiler, R. J. Cava and A. B. Bocarsly, *J. Am. Chem. Soc*., 2014, **136**, 830-833.

7 M. T. Mayer, C. Du and D. Wang, *J. Am. Chem. Soc*. 2012, **134**, 12406.

8 N. J. Cherepy, D. B. Liston, J. A. Lovejoy, H. M. Deng, J. Z. Zhang, *J. Phys. Chem. B*, 1998, **102**, 770. J. K. Leland and A. Bard, *J. Phys. Chem*., 1987, **91**, 5076.

9 M. A. Lukowski and S. Jin, *J. Phys. Chem. C*, 2011, **15**, 12388. A. Kay, I. Cesar and M. Grätzel, *J. Am. Chem. Soc*. 2006, **128**, 15714. Y. C. Ling, G. M. Wang, D. A. Wheeler, J. Z. Zhang and Y. Li, *Nano Lett*. 2011, **11**, 2119.

10 L. Wang, C. Y. Lee, P. Schmuki, *Electrochemistry Communications*, 2013, **30**, 21.

11 L. Wang, C. Y. Lee, A. Mazare, K. Y. Lee, J. Müller, E. Spiecker and P. Schmuki, *Chem. Eur. J*. 2014, **20**, 77.

12 N. T. Hahn and C. B. Mullins, *Chem. Mater*. 2010, **22**, 6474.

13 K. Sivula, R. Zboril, F. L. Formal, R. Robert, A. Weidenkaff, J. Tucek, J. Frydrych and M. Grätzel, *J. Am. Chem. Soc*. 2010, **132**, 7436.

14 Y. Q. Sun, W. D. Chemelewski, S. P. Berglund, C. Li, H. C. He, G. Q. Shi and C. B. Mullins, *ACS Appl. Mater.& Interfaces*, 2014, **6**, 5494.

15 R. L. Spray, K. S. Choi, *Chem. Mater*., 2009, **21**, 3701.

16 I. Herrmann-Geppert, P. Bogdanoff, J. Radnik, S. Fengler, T. Dittrichd and S. Fiechter, *Phys. Chem. Chem. Phys*., 2013, **15**, 1389.

17 Y. S. Hu, A. Kleiman-Shwarsctein, A. J. Forman, D. Hazen, J. N. Park and E. W. McFarland, *Chem. Mater*. 2008, **20**, 3803.

18 S. Tilley, M. Cornuz, K. Sivula, M. Grätzel, *Angew. Chem*., 2010, **122**, 6549. *Angew. Chem. Int. Ed*., 2010, **49**, 6405.

19 X. P. Qi, G. G. She, X. Huang, T. P. Zhang, H. M. Wang, L. X. Mu, W. S. Shi, *Nanoscale*, 2014, **6**, 3182.

20 B. Klahr, S. Gimenez, F. Fabregat-Santiago, J. Bisquert, and T. W. Hamann, *J. Am. Chem. Soc*. 2012, **134**, 16693.

21 X. P. Qi, G. G. She, M. Wang, L. X. Mu, W. S. Shi, *Chem. Commun*., 2013, **49**, 5742.

22 D. D. Qin, C. L. Tao, S. In, Z. Y. Yang, T. E. Mallouk, N. Z. Bao and C. A. Grimes, *Energy Fuels*, 2011, **25**, 5257.

23 W. R. Cheng, J. F. He, Z. H. Sun, Y. H. Peng, T. Yao, Q. H. Liu, Y. Jiang, F. C. Hu, Z. Xie, B. He and S. Q. Wei, *J. Phys. Chem. C*, 2012, **116**, 24060.

24 N. Mirbagheri, D. G. Wang, C. Peng, J. Q. Wang, Q. Huang, C. H. Fan and E. E. Ferapontova, *ACS Catal*. 2014, **4**, 2006.

25 L. Steier, I. Herraiz-Gardona, S. Gimenez, F. Fabregat-Santiago, J. Bisquert, S. D. Tilley and M. Grätzel, *Adv. Funct. Mater*. **2014**, *24*, 7681–8688